Supplementary Information

A polydimethylsiloxane coated metal structure for all-day radiative cooling

Lyu Zhou[1,*], Haomin Song[1,2*], Jian-Wei Liang[2,*], Matthew Singer[1], Ming Zhou[3], Edgars Stegenburgs[2], Nan Zhang[1], Chen Xu[4], Tien Khee Ng[2], Zongfu Yu[3,†], Boon Ooi[2,†], Qiaoqiang Gan[1,†]

1 *Department of Electrical Engineering, The State University of New York at Buffalo, Buffalo, NY 14260, USA.*

2 *Photonics Laboratory, King Abdullah University of Science and Technology (KAUST), Thuwal 23955-6900, Saudi Arabia*

3 *Department of Electrical and Computer Engineering, University of Wisconsin, Madison, Wisconsin 53705, USA*

4 *School of Life Information Science and Instrument Engineering, Hangzhou Dianzi University, Hangzhou 310018, Zhejiang Province, China*

* These authors contribute equally to this work.

† Email: zyu54@wisc.edu; boon.ooi@kaust.edu.sa; qqgan@buffalo.edu

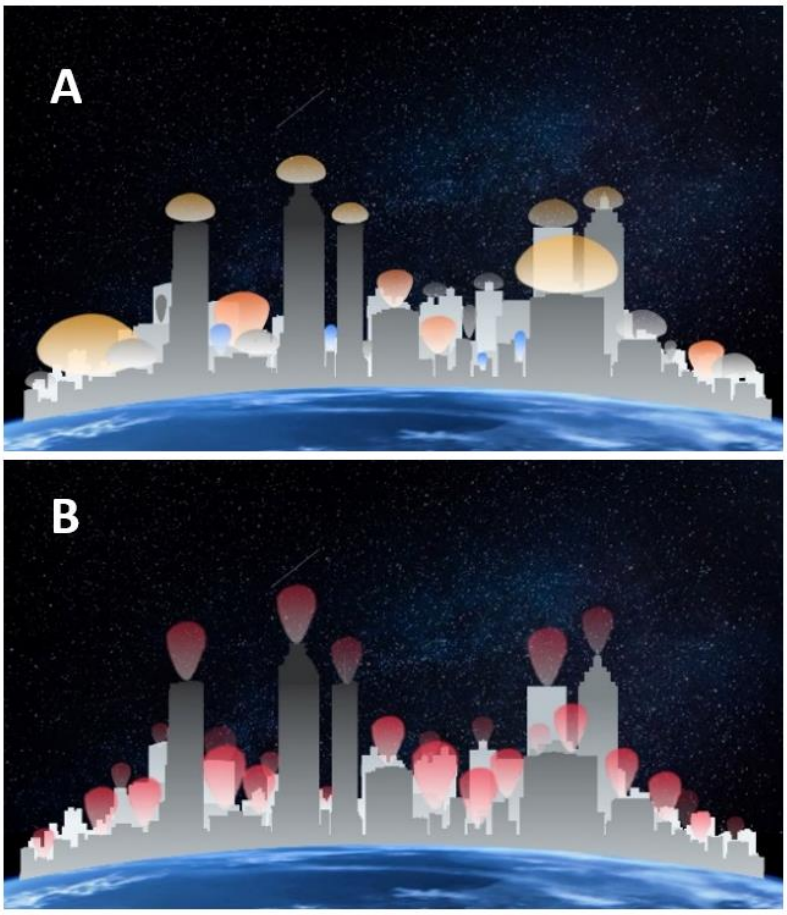

Supplementary Figure 1. Schematic illustration of radiative cooling in crowded urban area.

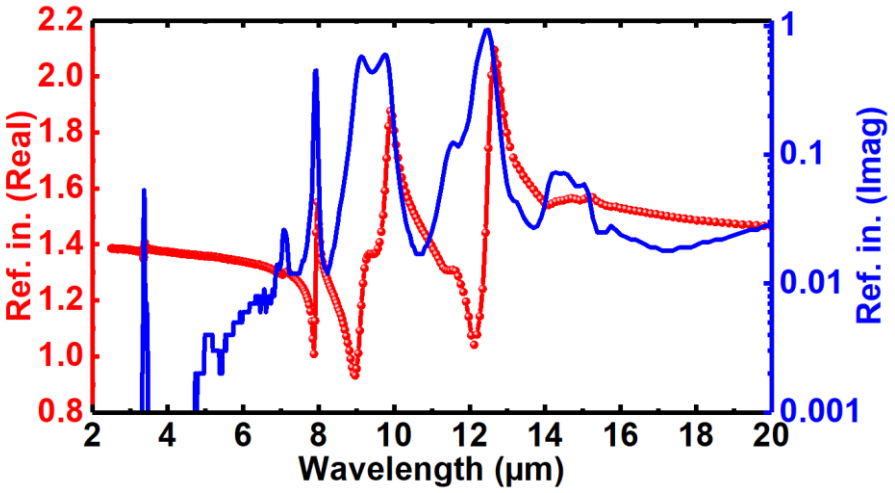

Supplementary Figure 2. The real part (red sphere) and imaginary part (blue line) of the effective refractive indices for PDMS layers. [S1]

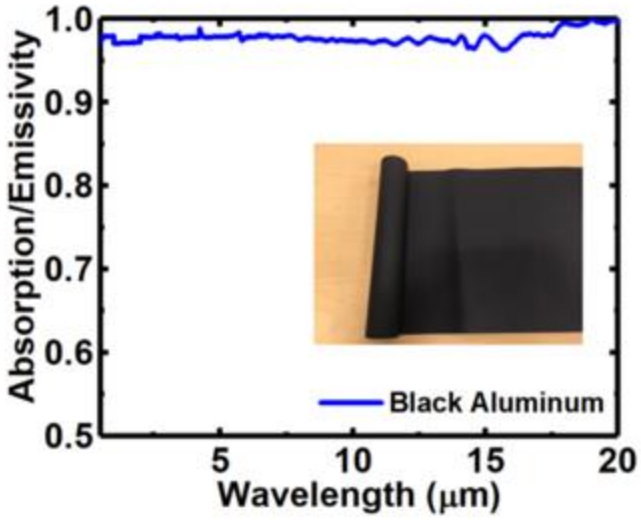

Supplementary Figure 3. Measured absorption spectrum of the Black aluminum cinefoil (Rosco Matte). The inset shows the photograph of the Black aluminum cinefoil.

Supplementary Figure 4. A photograph of the experimental setup without the beaming structure tested at Buffalo, NY.

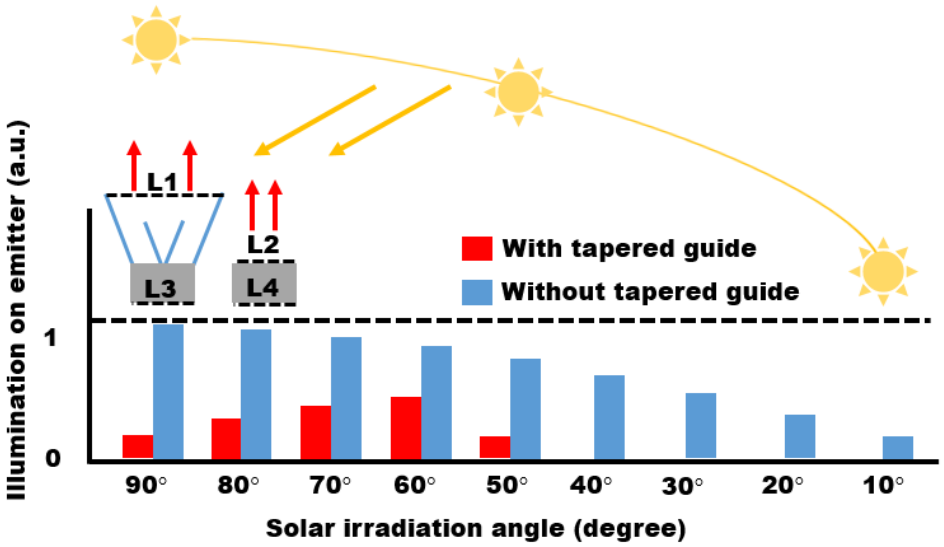

Supplementary Figure 5. Simulation results of solar illumination on emitters with and without the tapered guide. This simulation was performed using LightTools to study the solar light absorption of the tapered guide as the function of the incident angle.

Supplementary Figure 6. A photograph of the out-door test performed at King Abdullah University of Science and Technology (KAUST), Saudi Arabia.

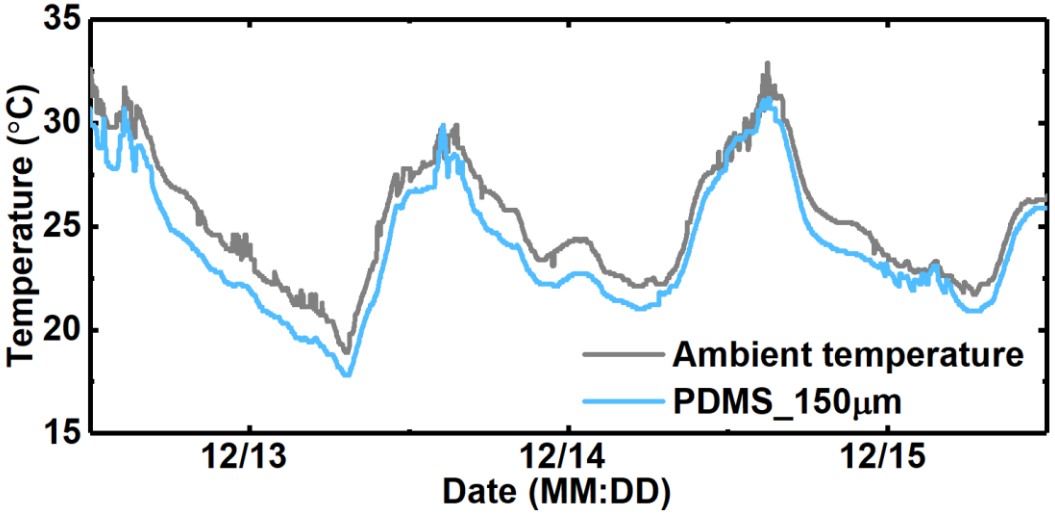

Supplementary Figure 7. The continuous radiative cooling test at Saudi Arabia. The relative humidity of the local test environment was ~60% at nighttime and ~50% during the daytime.

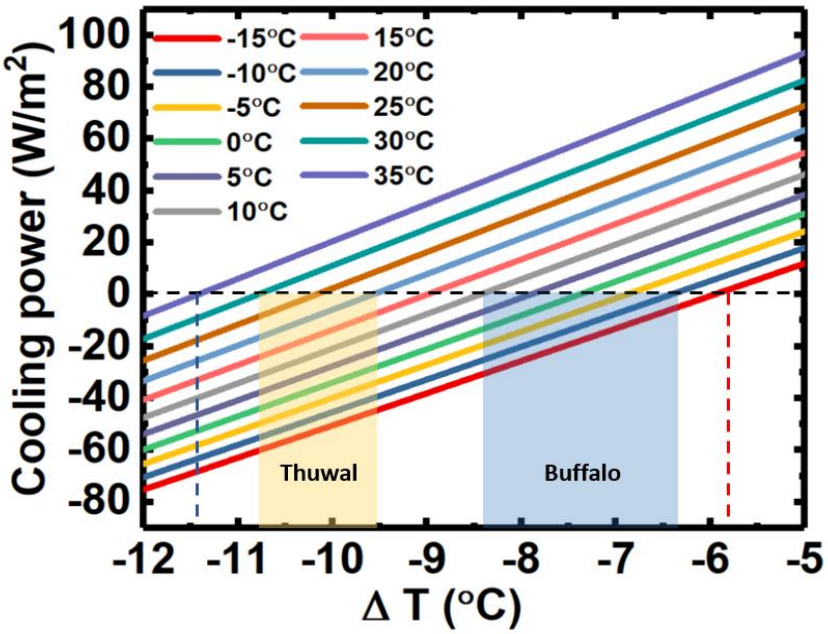

Supplementary Figure 8. The influence of ambient temperature over the net cooling power. The black dashed line indicates the temperature reduction (i.e., $\Delta T=T_{dev}-T_{amb}$) at the steady state. It should be noted that under this ideal estimation, ΔT obtained at Thuwal should be better than that at Buffalo due to the higher ambient temperature. However, the cooling power is heavily dependent on the actual environment condition, as we explained in Note S5.

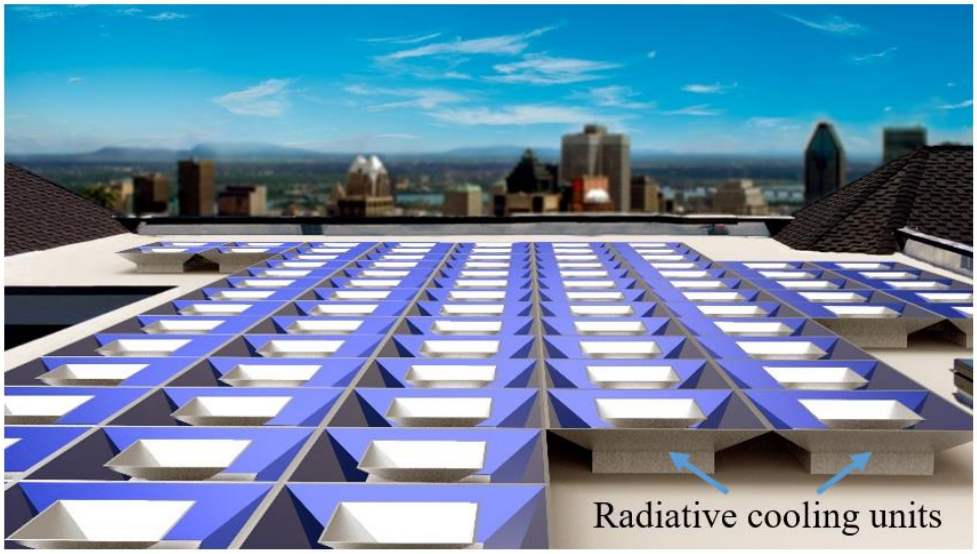

Supplementary Figure 9. Schematic illustration of modularized radiative cooling unit with beaming architectures.

Supplementary Notes 1. Radiative cooling in metropolitan areas

As illustrated in **Fig. S1a**, since the thermal emission is omnidirectional, only the roofs of those highest buildings can have the access to the complete clear sky. Thermal emission from short buildings will be blocked by their surrounding architectures, resulting in their limited accesses to the open sky. Therefore, a beam-controlled design is highly desired for enhanced radiative cooling architecture by manipulating the divergence angle of the thermal emission. Due to the enhance directionality of the thermal emission (**Fig. S1b**), the dependence of the radiative cooling performance on the surrounding environment can be minimized, addressing the practical implementation barrier for radiative cooling technology in crowded building environment.

Supplementary Notes 2. Indoor radiative cooling experiment

We developed an apparatus to perform radiative cooling experiment in the indoor environment. In general, the temperature of the outer space is usually considered as 3 K. However, a clear sky is not accessible in many areas due to the weather condition. In the indoor test, we employed a liquid nitrogen-immersed black aluminum as the cold source. A thermal insulating foam tank (350 mm* 250 mm* 250 mm) was wrapped by black aluminum foils (see Fig. S2 for its absorption spectrum). The tank was then filled with liquid nitrogen (LN2) with the temperature at 77K under the steady state. As shown by Figs. 2A and 2B in the main text, the PDMS/metal emitter was placed in a polystyrene foam box sealed by the polyethylene film. The foam box was then aligned with the cold source by an aluminum waveguide with the cross-sectional dimension of 260 mm×260 mm. The collection angle of the waveguide can be tuned by changing the height of the waveguide (see Fig. 2A in the main text).

To reveal the physical mechanism of the temperature reduction in the foam box, we employed two different thermocouples (D2, D3) to measure the environment temperature near the foam box and the ambient temperature. As indicated in Fig. 2A in the main text, D2 was placed on the edge of the foam box and D3 was placed at a place far from the apparatus. The temperature of two thermocouples (shown by black and grey lines in Fig. 2D) were almost identical. This result indicates that the air gap between the LN2 tank and the foam box is sufficient to suppress the heat exchange through convection/conduction channels. Therefore, thermal radiation is the only heat channel responsible for the temperature reduction inside the foam box.

Supplementary Notes 3. Calculation of the radiative cooling power

Here we analytically analyze the cooling power of the emitter using Eq. (1) in the main text.

Given an area of A, the radiative cooler can possess the net cooling power P_{net}, which is given by Eq. (1) in the main text. In this equation, the thermal radiation $P_{rad}(T_{dev})$ emitted by the emitter is:

$$P_{rad}(T_{dev}) = \int d\Omega \cos(\theta) \int d\lambda I_{BB}(T_{dev}) \varepsilon_{dev}(\theta, \lambda) \quad \text{(S1)},$$

where T_{dev} is the temperature of the emitter; $\int d\Omega = 2\pi \int_{\theta_1}^{\theta_2} d\theta \sin\theta$ is the angular integral of the emitter over the space, θ_1 and θ_2 are defined by the testing environment. $I_{BB}(T) = \frac{2hc^2}{\lambda^5} \frac{1}{\exp\left(\frac{hc}{\lambda k_B T}\right) - 1}$ is the spectral radiance of a blackbody at the temperature T; ε_{dev} is the spectral emissivity of the emitter (here we replaced

it with the measured absorption using Kirchhoff's radiation law). h is the Planck's constant; k_B is the Boltzmann constant; c is the speed of light and λ is the wavelength.

The incident radiation powers from the ambient, P_{amb}, and from the cold source, $P_{cold\ source}$, are given by the following two equations, respectively:

$$P_{amb}(T_{amb}) = \int d\Omega \cos(\alpha) \int d\lambda I_{BB}(T_{amb}) \varepsilon_{dev}(\theta, \lambda) \varepsilon_{air}(\alpha, \lambda) \quad \text{(S2)}$$

$$P_{cold\ source} = \int d\Omega \cos(\beta) \int d\lambda I_{BB}(T_{cs}) \varepsilon_{dev}(\theta, \lambda) \varepsilon_0(\beta, \lambda) \quad \text{(S3)},$$

where the angular-dependent emissivity of atmosphere $\varepsilon_{air}(\alpha, \lambda)$ is given by $\varepsilon_{air}(\gamma, \lambda) = 1 - [1 - \varepsilon_{air}(0, \lambda)]^{\frac{1}{\cos\gamma}}$. $\varepsilon_0(\beta, \lambda)$ is the emissivity of the cold source. T_{amb} is the temperature of the ambient air; T_{cs} is the temperature of cold source;

The last term of Eq. (1), $P_{nonrad}(T_{dev}, T_{amb})$, is the nonradiative power loss introduced by convection and conduction, which is given by

$$P_{nonrad}(T_{dev}, T_{amb}) = q(T_{dev} - T_{amb}) \quad \text{(S4)}.$$

Here q is the conduction/convection efficiency. In the indoor experiment, the q was set to 10 W m^{-2}K^{-1} (e.g. ref. [28]).

To estimate the radiation cooling power of the PDMS/metal emitter, we followed the procedure outlined in a previous work [10], where the cooling power of the system at ambient temperature can be defined as the net power when the emitter is at the ambient temperature. In our case, the measured ambient temperature is 288 K. As a result, one can obtain that the net power P_{net} is 122.647 W/m^2, P_{rad} is 245.3413 W/m^2, P_{amb} is 122.4640 W/m^2, $P_{cold\ source}$ is 0.0303 W/m^2 and P_{nonrad} is 0.

It should be noted that in the indoor experiment, the cold source is the black aluminum immersed in liquid nitrogen (77K) which is much higher than the cold source in the outer space (3K). According to the data we calculated above, the radiation power of the cold source at 77K is only 0.0303 W/m^2, which is negligible compared to the net power of 122.647 W/m^2. Therefore, the black aluminum immersed in liquid nitrogen is an ideal alternative to serve as the cold source to validate the radiative cooling performance in the laboratory.

Supplementary Notes 4. Analysis of the cooling performance in the outdoor test

For the outdoor test, the radiative cooling power analysis of the emitter is the same as the one outlined in Note S2. However, since the test environment gets complicated, more environmental factors have to be considered (e.g., influence of the solar irradiation; weather conditions like humidity, wind speed, cloud distribution; and the angular response of atmospheric transmission [S2, S3]). Here we will theoretically discuss the variation of the cooling power under different ambient temperature.

Using Eqs. (1) and S1-S4, we modeled the cooling power vs the temperature reduction, as shown in **Fig. S7**. The room temperature was tuned from -15 °C to 35 °C, which should cover the annual temperature range at Buffalo, USA. The intersection points with the dashed line for P_{net}*=0 W/m^2* indicate the temperature reduction of the steady state. One can see that the reduced temperature (ΔT) is indeed dependent on the ambient temperature. As the ambient temperature increases, the temperature reduction should be larger, indicating a better cooling performance. However, even T_{amb} changes from 35 ºC to -15 ºC (a difference of 50 ºC), the ΔT changes by only ~5.4 ºC. To reveal the influence of the ambient temperature on the

outdoor cooling performance, we highlighted the two shadow areas in Fig. S7. At Buffalo, the ambient temperature varies from -10 °C to 10 °C as shown in Fig. 5B in the main text, resulting in ~2.0 °C difference in ΔT; while at Thuwal, the ambient temperature varies from 20 °C to 30 °C, resulting in ~1.2 °C difference in ΔT.

Supplementary Notes 5. The effect of the tapered spectrum selection architecture

The tapered guide was implemented to beam the thermal radiation and block the solar irradiation. The absorption spectrum of the spectrum selective material is shown in Fig. 4A in the main text. Here we employed a simplified ray tracing model to estimate the solar illumination and thermal emission loss introduced by this tapered structure.

Solar absorption: The solar absorption is related to the incident angle of sun light, as shown in **Fig. S4**. We modeled the solar powers absorbed by surfaces L3 and L4, respectively. One can see that most of the solar energy will be filtered with the spectrum selective architecture. For example, for an incident angle of 90°, the solar light reaching the emitter surface with the tapered guide is only 17.9% compared to the one without the beaming architecture. When the incident angle is tuned to 60° (corresponding to the angle of the tapered architecture), a part of the solar light can directly illuminate L3, ending up with an increased illumination on emitter. As the incident angle reaches 40° and below, the tapered guide can block all incident solar energy, while the system without the taper structure still absorbs a significant amount of the incident solar energy. For instance, when the incident angle is 40°, the solar absorption of the thermal emitter in the control system is 64.2% of its peak absorption obtained under the angle of 90°.

Thermal emission: To model the thermal emission with and without the tapered architecture, a uniform light source was set on L3 and L4. We then calculated the powers through L1 and L2, respectively, and revealed that the thermal emission power on L1 was 85.1% of that on L2. Therefore, the thermal loss introduced by the tapered guide is 14.9%. Therefore, the cooling performance with the tapered architecture is slightly lower than the control system without beaming effect. The next step investigation should be the optimization of the spectral selection feature of the material used for the beaming architecture, which is still under investigation and will be discussed elsewhere.

Supplementary Notes 6. Radiative cooling test at Thuwal, Saudi Arabia

Another outdoor cooling test was performed at Thuwal, Saudi Arabia to study how weather conditions would affect the performance of PDMS/metal emitter. The test data was collected from December 13th 2017 to December15th 2017. The ambient temperature was from 18 °C to 32 °C with the relative humidity of 50%~60%. In addition, the visibility at Thuwal was ~10 km (due to a light sand storm during this period of time). In contrast, the visibility at Buffalo area was ~ 16 km. As shown in Fig. S6, the temperature reduction was < 3 °C, which is far below the theoretical calculation shown in Fig. S7 estimated under this high temperature environment. The major mechanism should be attributed to the dust in the sky, blocking the pathway of the thermal radiation. In addition, the high relative humidity could also be one of the major reasons (e.g. [S2]). In this high-temperature environment, the high relative humidity indicates a higher moisture capacitance per unit air volume, resulting in a lossy channel in the 8-14 μm window.

Supplementary References

S1. A. Srinivasan, B. Czapla, J. Mayo, A. Narayanaswamy, Infrared dielectric function of polydimethylsiloxane and selective emission behavior. *Applied Physics Letters* **109**, 061905 (2016).

S2. C. Y. Tso, K. C. Chan, C. Y. H. Chao, A field investigation of passive radiative cooling under Hong Kong's climate. *Renewable Energy* **106**, 52-61 (2017).

S3. G. B. Smith, Amplified radiative cooling via optimised combinations of aperture geometry and spectral emittance profiles of surfaces and the atmosphere, Solar Energy Materials and Solar Cells, **93**, 1696-1701 (2009)